On the High Load Limit of Boosted Gasoline HCCI Engine Operating in NVO mode

Citation: Scaringe, Robert, Craig Wildman, and Wai K. Cheng. On the High Load Limit of Boosted Gasoline HCCI Engine Operating in NVO Mode. SAE International Journal of Engines, 3(1):35-45, 2010.

As Published: http://dx.doi.org/10.4271/2010-01-0162

Publisher: SAE International

Persistent URL: http://hdl.handle.net/1721.1/66905

Version: Author's final manuscript: final author's manuscript post peer review, without publisher's formatting or copy editing

On the High Load Limit of Boosted Gasoline HCCI Engine Operating in NVO mode

Robert J. Scaringe, Craig B. Wildman, Wai Cheng
Massachusetts Institute of Technology

ABSTRACT

The high load limit of a boosted homogeneous-charge-compression-ignition (HCCI) engine operating on negative-valve-overlap (NVO) was assessed. When operating under stoichiometric condition with no external dilution, the load, as measured by the net indicated mean effective pressure (NIMEP), increased with increase in manifold absolute pressure (MAP), and with decrease in trapped amount of residual gas. The maximum pressure rise rate (MPRR), however, also increased correspondingly. When the MAP and the amount of residual gas were adjusted so that the engine operating point could be held at a constant MPRR value, the NIMEP increased with the simultaneous decrease in MAP and residual until the misfire limit was reached. Therefore if a MPRR ceiling is imposed, the high load limit of an HCCI engine is at the intersection of the constraining MPRR line and the misfire line. Dilution with cooled exhaust gas recirculation (EGR) shifted both the MPRR line and the misfire line so that the intersection point would be at a higher MAP and a higher level of dilution. The NIMEP value at this new intersection point, however, did not change substantially. Thus using cooled EGR dilution strategy, the MPRR constrained high load limit is approximately neutral to boosting.

INTRODUCTION

Gasoline homogeneous-charge-compression-ignition (HCCI) engines could offer substantial gain in fuel economy [1]. The operating range, however, is rather limited with respect to driving requirements [2, 3]. Consequently, there is significant interest in extending the HCCI engine load range. Since at the same stoichiometric ratio, the amount of fuel burned is proportional to the amount of air trapped in the cylinder, boosting should, in principle, increase the engine output load (as measured by the Net Indicated Mean Effective Pressure –NIMEP). In practice, the Noise-Vibration-Harshness (NVH) and engine durability concerns pose a significant limit on the high load limit of boosted HCCI engines [4-8].

This paper concerns the high load limit of operating an HCCI engine with boosting. It is a continuation of the previous work [4] in studying the high load limit of a boosted single cylinder HCCI engine operating in the negative-valve-overlap (NVO) mode using electromagnetically activated intake and exhaust valves. In that work, the maximum pressure rise rate (MPRR) was used as a metric for NVH. External cooled exhaust gas recirculation (EGR) was found to be effective in reducing MPRR in a boosted engine. However, the trapped charge temperature also decreased with EGR so that at some point, the charge was not hot enough for HCCI, and the engine misfired. Therefore, it is of interest to understand the relationship between the high load NVH limit and the misfire limit in a boosted HCCI engine operating with NVO.

The scope of this paper is as follows:

(i) To determine the gross impact of the engine operating variables on HCCI engine MPRR.
(ii) To assess the impact of cooled EGR on the HCCI engine misfire limit at high load (here and in subsequent references, load is measured by the NIMEP value).
(iii)To understand the relationship between the high load limit and misfire limit, and the impact of EGR on the MPRR-constrained high load limit.

EXPERIMENTAL SET UP AND TEST CONDITIONS

The details of the engine with an electromagnetically activated variable valve timing system [2] and the intake system with boost and cooled EGR [4] have been reported previously. The experimental set up is briefly described here for completeness. The engine and fuel parameters are shown in Table 1.

Table 1 Engine and Fuel Parameters

Bore	80.26 m
Stroke	88.9 mm
Connecting rod	158 mm
Displacement	449.8 cc
Compression ratio	10.2
Fuel	Certification fuel UTG91
Octane #	RON 91, MON83
Injection pressure differential for PFI	2.7 bar

The engine used a Ricardo Hydra Diesel Crankcase and a VW TDI (model year 2001) head. Fuel is introduced by port fuel injection. The original diesel injector was replaced by a small racing car spark plug. Pressure was measured by a Kistler 6125 transducer through the original glow plug hole.

The boosted air supply and cooled EGR system are shown in Fig. 1. The compressor was a production supercharger from a BMW Minicooper vehicle, and was driven by an electric motor. The manifold absolute pressure (MAP) could be adjusted up to 1.7 bar by varying the motor drive speed. The exhaust pressure was maintained by a close-loop controlled throttle to be 0.03 bar above MAP to enable EGR. The EGR was water cooled. The EGR temperature was above the dew point to prevent water condensation. The cooled EGR flow was then reheated to the same temperature of the fresh air, which was also temperature controlled by a heater.

The amount of EGR was determined by a CO_2 measurement at the intake port and in the exhaust line. The in-cylinder residual gas fraction was determined by the exhaust temperature and pressure measurements; the method had been verified by direct in-cylinder CO_2 sampling measurement using a fast CO_2 meter from Cambustion Ltd. as described in a previous study [4].

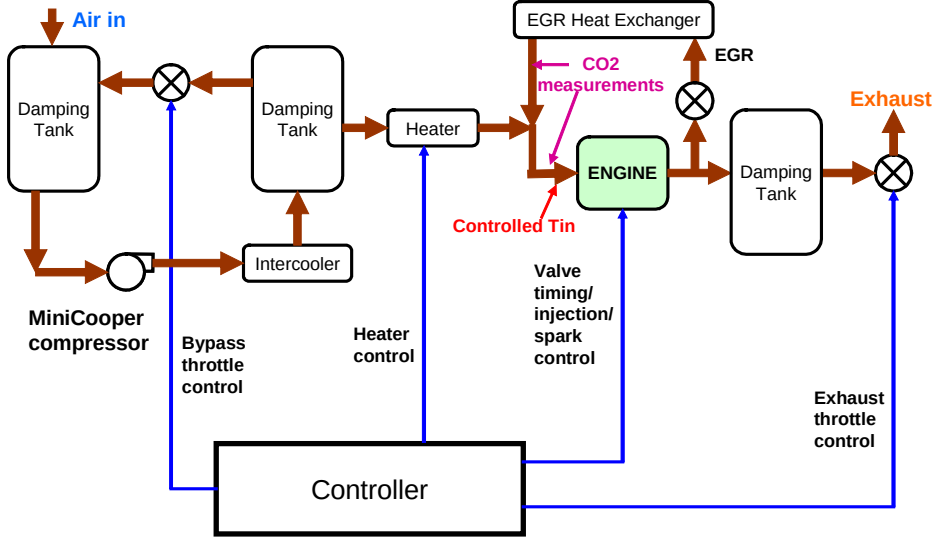

Fig. 1 Engine set up for boosted operation with cooled EGR

The valve timing strategy is shown in Fig.2. The timings for IVC and EVO were fixed (see Fig.2 caption for values). The timings for EVC and IVO were set symmetric with respect to TDC-intake so that the amount of negative overlap was determined by the NVO half angle θ_0; the amount of NVO determined the amount of trapped burned gas retained for next cycle.

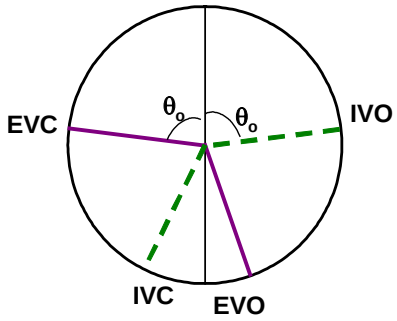

Fig.2 Valve timing strategy: IVC fixed at 29^o ABC-compression; EVO fixed at 15^o BBC-expansion; NVO symmetric about TDC exhaust; NVO half angle is θ_0.

All the data were taken at the engine speed of 1500 rpm with a stoichiometric mixture except for the experiments which compared the dilution by burned gas and by air, for which there was excess air. The exhaust pressure was set to MAP+0.03 bar. The amount of EGR was set by the EGR valve as shown in Fig. 1. The experimental parameters are shown in Table 2.

Table 2 Range of operating conditions

MAP	1 to 1.7 bar
Intake temperature	30 to 120^o C
EGR dilution without excess air (stoichiometric condition	0-30% by moles of EGR gas
Dilution with excess	0-30% by moles

air(lean condition)	of excess air
Residual burn gas	30 -60%, depending on NVO setting

HCCI ENGINE OPERATING VARIABLES IMPACT ON MPRR

A large data set was collected with the range of parameters varied according to Table 2. Some of the results were previously reported [4]. The task here is to develop a correlation based on that data so that the *gross* dependence of MPRR on engine operating condition could be established. We have put emphasis on the *gross* dependence because in general, the MPRR depends on the detailed charge temperature and concentration stratifications. As a matter of fact, stratification is often used as a strategy to control MPRR [9, 10]. Quantifying stratification is difficult since such data are difficult to generate and since a simple metric for stratification has not been devised. Furthermore, the spatial distribution changes during the engine process. Nevertheless, quantifying the gross dependence of MPRR on engine parameters, not withstanding the effects of stratification, is useful because such a correlation would give an estimate to the change in MPRR due to the gross change of operating condition (such as MAP or intake temperature), all other things kept "equal."

The pertinent observations from the data set are [4]:

(a) At fixed NVO, the NIMEP increased with MAP and decreased with intake temperature. The latter was a volumetric efficiency effect. The corresponding MPRR increased with both MAP and intake temperature.

(b) Comparing at the same total dilution (see Definition/Abbreviation section for detailed definition), dilution by EGR was effective in lowering MPRR by lowering the charge temperature. However, at high EGR level, the charge would be too cold for HCCI operation and led to misfire.

(c) With air dilution (operating lean at the same dilution ratio, intake temperature, and MAP), MPRR did not improve; instead, it deteriorated. The effect was due to the increase of oxygen concentration, which promoted reaction, and also to the increase in compression temperature due to the higher specific heat ratio.

Values of MPRR are plotted against NIMEP for all the data in Fig. 3. There was substantial data scatter. To interpret this data, the first law of thermodynamics was applied to the charge [4]:

$$\dot{p}=(\gamma-1)\left[\dot{q}-\frac{\dot{Q}_L}{V}\right]-\left(\gamma P\frac{\dot{V}}{V}\right) \quad (1)$$

(See Definition/ Abbreviation section for symbol definitions.) Since the heat loss and volumetric expansion terms are small compared to the volumetric heat release term, they may be dropped from Eq. (1); MPRR is then given by

$$\text{MPRR}=(\gamma-1)\left[\frac{m_f \text{LHV}}{V(\theta)\tau_{\text{reaction}}}\right]_{\max} \quad (2)$$

Here, the volumetric heat release rate $\dot{q}$ in Eq. (1) has been replaced by the average charge fuel energy density at the maximum pressure rise rate point, divided by an overall reaction time τ_{reaction}. To assess whether the data

supports an interpretation in the manner of Eq.(2), V(θ) is approximated by V(CA50), and $\tau_{reaction}$ by $\Delta\tau_{10\text{-}90}$. Then the relationship according to Eq. (2) is shown in Fig. 4. The significant reduction of the data scatter (compared to Fig. 3) indicates that Eq. (2) is indeed a valid assessment of the MPRR dependence.

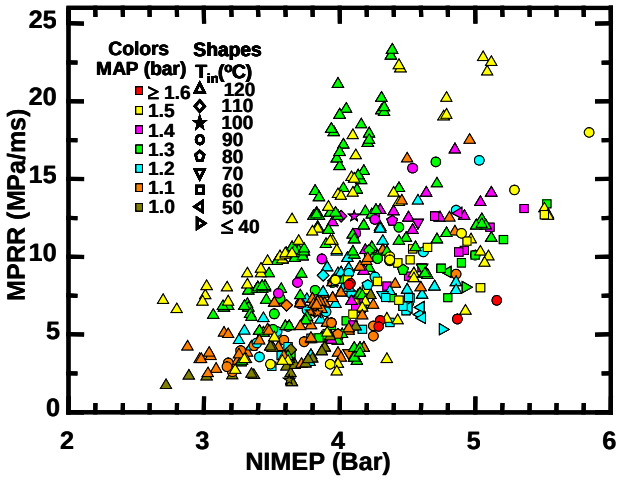

Fig. 3 NIMEP as a function of NIMEP. The colors and symbols represent different operating conditions. The dilution data with both EGR and air were included but not explicitly marked; from [4].

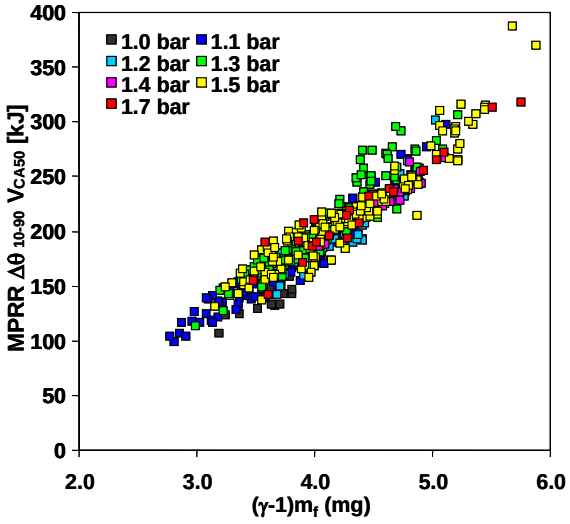

Fig. 4 Correlation plot of MPRR to engine parameters.

To make Eq.(2) a useful formula for assessing MPRR, instead of using $\Delta\tau_{10\text{-}90}$, the value of $\tau_{reaction}$ was calculated directly from the data:

$$\frac{1}{\tau_{reaction}} = \left[\frac{MPRR\ V(CA50)}{(\gamma-1)m_f LHV}\right]_{data} \quad (3)$$

This value was then regressed against the engine thermo-chemistry variables to produce the following correlation:

$$\left(\frac{1}{\tau_{reaction}}\right) = 3.32 \cdot x_{O2}^{1.88} \cdot x_{fuel}^{0.35} \cdot P_{10\ BTC}^{1.92} \cdot \exp\left(\frac{-2560}{T_{10\ BTC}}\right) \quad (4)$$

($\tau_{reacton}$ in ms; P in bar; T in K)

The choice of x_{O2} instead of the residual gas fraction as variable was to reflect the significant influence of oxygen concentration (see observation (c) above). The compression pressure and temperature at 10^{o} before-top-center were chosen as the thermodynamics variables because up to that point, there was no significant heat release, and the temperature and pressure there encompassed the effects of the trapped enthalpy of the residual, the intake air temperature, and the heat loss. The value of $T_{10\ BTC}$ was calculated from $P_{10\ BTC}$ using the ideal gas law and the residual fraction value obtained from the exhaust temperature and pressure measurements [4].

The result of the regression is shown in Fig. 5. The agreement was satisfactory ($R^2 = 0.71$). The data scatter (bracketed by a factor of 0.5 to 1.5) may be attributed to stratification effects and to error in the charge temperature estimate. Reported ignition delay data targeted to HCCI combustion conditions indicate that the reaction rate is highly sensitive to temperature [11]. Since the temperature estimate relies on the residual fraction estimate, even a small error from the calculation in the latter could result in significant scatter for the $1/\tau$ correlation of Eq. 4.For example, if the residual fraction is estimated to be 38% instead of 40% — a 5% error, which is realistic — the T_{10BTDC} value would be 27^{o} K lower. Then there will be a 44% decrease in ignition delay (using the correlation in [11] for iso-octane). Thus the data scatter in Fig. 5 is within the accuracy of the experiment.

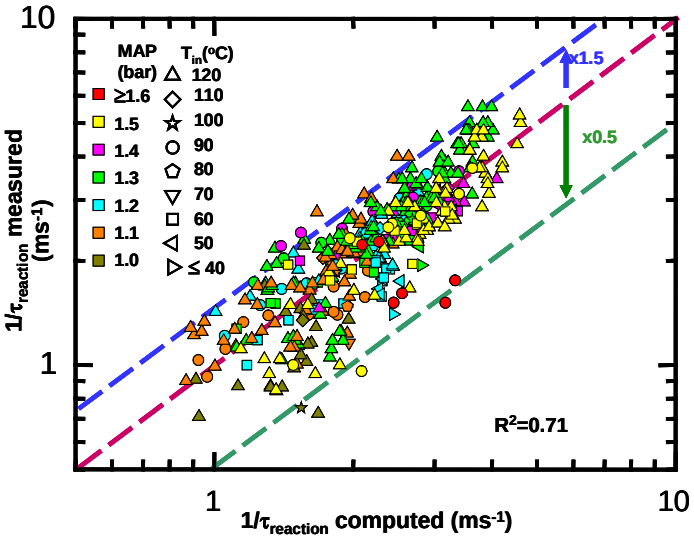

Fig. 5 Comparison between reaction rate obtained from data and from the correlation of Eq. (4).

To assess the stratification factors, it was noted that precise quantitative measures of stratification are difficult. Therefore, the following variables that addressed stratification were added to the regression:

(1) $(T_{exh} - T_{in})$; to represent the temperature non-uniformity due to the mixing between the hot trapped residual and the relatively cool intake fluid.
(2) $x_r\ (1- x_r)$; to represent the concentration non-uniformity due to the mixing between the residual and the fresh charge.

(3) $(1-x_{EGR})$; to represent the concentration non-uniformity due to the mixing between the recirculated exhaust gas and the fresh charge. (Strictly speaking, the expression should be x_{EGR} $(1- x_{EGR})$. However, a significant part of our data set was obtained with x_{EGR} =0, so such an expression would not work.)

It is recognized that the above variables did not address the stratification profiles, nor did they address any correlation between temperature and concentration stratifications. Nevertheless, assessing the regression by inclusion of these variables would give an indication of the effects of stratification.

The following correlation was obtained when the above "stratification" variables were added to the regression.

$$\left(\frac{1}{\tau_{reaction}}\right) = 4.93 \cdot x_{O2}^{\ 0.11} \cdot x_{fuel}^{\ 1.38} \cdot P_{10\ BTC}^{\ 2.55} \cdot \exp\left(\frac{-893}{T_{10\ BTC}}\right) (T_{exh} - T_{in})^{-1.63} [x_r(1-x_r)]^{-3.73} (1-x_{EGR})^{3.46} \qquad (5)$$

($\tau_{reacton}$ in ms; P in bar; T in ^oK)

(

The result of the regression with this expanded set of variables is shown in Fig. 6. Although the stratification variables were a very crude representation of stratification, the agreement improved significantly (R^2=0.87), thus giving support to the hypothesis that stratification did play a significant role in explaining the data scatter in Fig. 5.

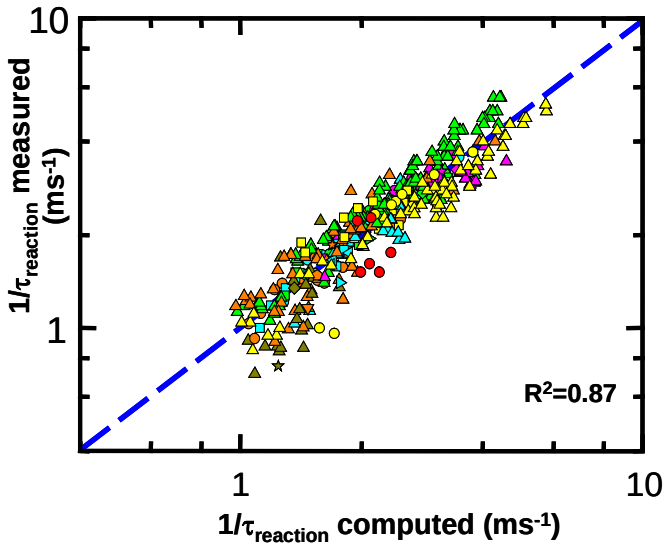

Fig. 6 Comparison between reaction rate obtained from data and from the correlation of Eq. (5)

In summary, an overall reaction rate $1/\tau_{reaction}$ may be related to the thermodynamics and mole fraction variables by the correlation of Eq. (4). Then the MPRR value may be calculated from Eq. 6.

$$MPRR=(\gamma-1)\left[\frac{m_f LHV}{V\,\tau_{reaction}}\right] \qquad (6)$$

Since the rapid pressure rise nominally occurs near TDC, the volume V at the maximum pressure rise rate point in Eq. (6) may be approximated by an average value, say V_{10}^{o}, the cylinder volume at 10^o after TDC. (For compression ratios of 10 to 15, the change of cylinder volume respect to V_{10}^{o} is less than 15% from TDC to 15^o

after TDC.) The utility of Equations (4) and (6) is that they provide a reasonable assessment of the scaling of MPRR when the engine operating condition changes, not withstanding the stratification effects.

IMPACT OF EGR ON HCCI ENGINE MISFIRE LIMIT AT HIGH LOAD

Exhaust gas recirculation was found to be effective in suppressing MPRR. However, EGR displaces air so that for a given value of MAP and NVO setting, the load will decrease. If the NVO is adjusted so that the amount of burned gas (residual plus EGR) is kept constant, the temperature of the trapped charge will decrease as EGR increases. At some point, the charge temperature will be insufficient to sustain HCCI operation and the engine will misfire.

To assess the interactions between MPRR, NIMEP, and misfire in an HCCI engine near the high load limit, the engine behavior was mapped extensively at selected values of MAP and intake fluid temperature. The air/fuel ratio was set to stoichiometric. In this process, the valve timing was set, and the EGR valve and the exhaust throttle valve (see Fig. 1) were adjusted to vary the EGR level while keeping the exhaust pressure at 0.03bar above the MAP. EGR flow was increased until the engine misfired. The misfire points were defined as where the engine would still run stably, but an increase in EGR flow would lead to unstable operation. (At the latter setting, the engine could run for a short time before erratic behavior characterized byvery large cycle-to-cycle fluctuations led to death.) A typical map of MPRR and misfire limit is shown in Fig. 7. The horizontal axis of the contours is the total burned gas fraction, x_{burn}, in the unburned charge ($x_{burn} = x_r + x_{EGR}$). The value was varied by the combination of EGR valve and NVO settings. The vertical axis is the fraction of EGR in the burned gas. The MPRR values decreased with both increase of x_{burn} and of the EGR fraction in the burned gas.

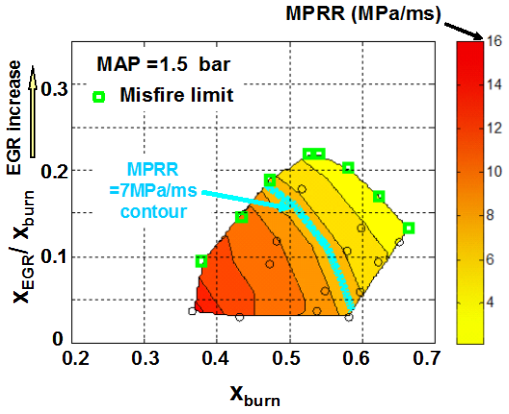

Figure 7 Map of MPRR and misfire limit at MAP = 1.5 bar; $\lambda = 1$. The markers are the mapped points, the data from which the contour map was constructed.

The corresponding map of NIMEP and misfire limit is shown in Fig. 8. The NIMEP values were mainly a function of x_{burn} (NIMEP increase with decrease of x_{burn}) and not sensitive to the EGR fraction. The slight dependence of the latter was due to the variation of fuel conversion efficiency.

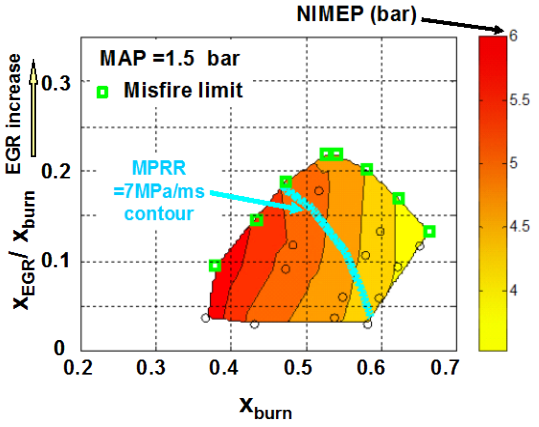

Fig. 8 Map of NIMEP and misfire limit at MAP = 1.5 bar; λ = 1. The markers are the mapped points, the data from which the contour map was constructed.

The relationship between the engine variables at the misfire limit was sought. The range of data encompassed MAP from 1.1 to 1.7 bar, and intake fluid temperature from 60 to 150° C. The regressed variables were x_{O2}, x_r, T_{in}, and MAP. The following correlation was obtained.

$$x_{O_2} = 3.036\, x_r^{-0.978} T_{in}^{-0.693} MAP^{-0.428} \quad (7)$$

The result of the regression is shown in Fig. 9. The agreement was excellent ($R^2 = 0.997$). The very tight correlation indicates that, unlike the overall reaction rate ($1/\tau_{reaction}$ in Eq. (4), which determines MPRR), the misfire limit was predominately determined by the overall thermodynamics variables and the residual gas fraction; it was not sensitive to stratification.

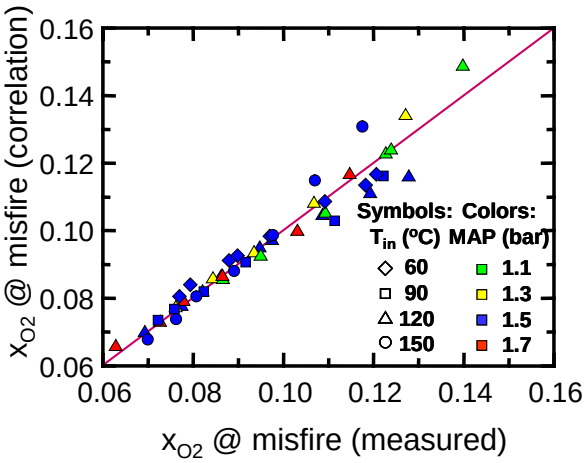

Fig. 9 Comparison between measured x_{O2} at misfire limit and computed value according to Eq. (7)

HIGH LOAD LIMIT, MISFIRE LIMIT, AND INFLUENCE OF EGR

To understand the relationship between NIMEP and MPRR under different engine settings of MAP, residual gas fraction, and EGR, the topology of the NIMEP and MPRR contours are examined as a function of the mole fraction of unburned charge oxygen x_{O2} and MAP. The use of x_{O2} as a governing parameter is because of its significant influence on MPRR (see discussion immediately after Eq. (4)). The value of x_{O2} can easily be calculated from the mole fractions of residual (x_r) and EGR (x_{EGR}); see Appendix A.

For the case of no EGR, a typical contour map in the x_{O2}-MAP diagram is shown in Fig. 10 with the misfire boundary. The NIMEP increased with both MAP and x_{O2}; the constant NIMEP contours were therefore lines of negative slopes. The MPRR also increased with both MAP and x_{O2}; thus the MPRR contours were also lines of negative slopes. It is shown in Appendix B that the MPRR contour lines are always steeper (more negative) than the NIMEP contour lines. This observation has a significant implication on the high load operating limit.

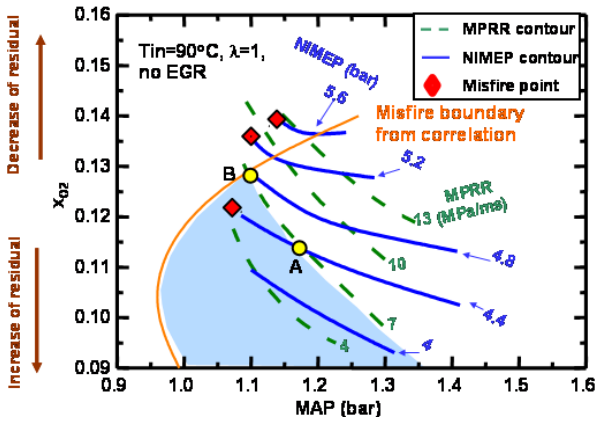

Fig. 10 MPRR/ NIMEP contours and misfire boundary on the x_{O2}-MAP diagram; T_{in} = 90° C, λ =1, no EGR. Both the actual misfiring point and the misfire boundary according to the correlation of Eq. (7) are shown. Shaded area is the permitted region of operation under MPRR constrain of 7 MPa/ms.

For illustrative purpose, assume that the MPRR value is constrained at 7MPa/ms. Then, the MPRR constraint and the misfire constraint will limit the operating domain to be in the shaded area in Fig. 10. If, for example, the operating point is at A (4.4 bar NIMEP), then because that the MPRR contours are steeper than the NIMEP contours, the NIMEP could always be increased by shifting the operating point to the left along the MPRR contour until the misfire limit is reached (point B, at NIMEP of 4.8 bar). Thus for MPRR constrained operation, the maximum NIMEP occurs at the intersection between the MPRR constraint line and the misfire boundary. Hence, the high load limit and the misfire limit coincide under the MPRR constraint.

If EGR is used, both the MPRR contour and the misfire boundary will move. The NIMEP contours will mainly depend on the amount of fuel burned (with modification due to change in fuel conversion efficiency) and thus do not change much on the x_{O2}-MAP diagram. The typical situation is shown in Fig. 11.

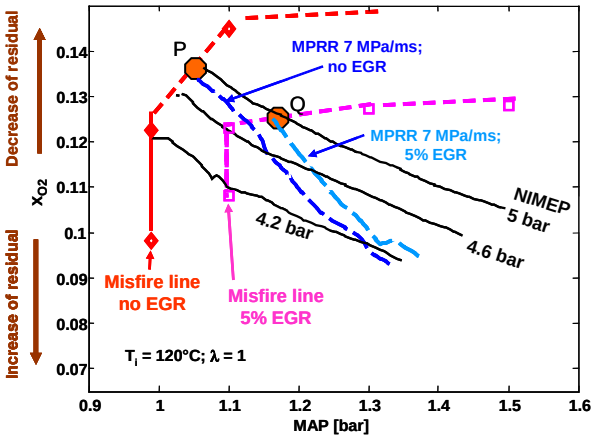

Fig. 11 MPRR, NIMEP contours and misfire boundary on the x_{O2}-MAP diagram, showing effect of EGR; T_{in} = 120° C, λ =1.

The effects of increasing EGR from 0 to 5% (operating at $\lambda = 1$) on the MPRR/ NIMEP contours and misfire boundary are shown in Fig. 11. The NIMEP contours did not change materially. The MPRR contours shifted up and to the right; thus at the same burned gas fraction in the unburned mixture (same x_{O2}), the engine could be operated at a higher MAP with the same MPRR. The misfire boundary, however, shifted down and to the right. The net effect on maximum NIMEP may be illustrated with the example of using the constrain of MPRR = 7 MPa/ms. Then the high load limit is at point P (intersection of the MPRR = 7 MPa/ms contour and the misfire boundary) for 0% EGR, and at point Q for 5% EGR. These two points have approximately the same NIMEP even though they are operating at different MAP values.

The change in maximum load under the MPRR constrain of 7 MPa/ms as a function of EGR is shown in Fig. 12. For EGR increase from 2.5 to 21%, the maximum NIMEP only changed modestly (from 5.1 bar to 5.7 bar), although the MAP had increased from 1.1 to 1.7 bar. Thus the MPRR constrained maximum load is roughly neutral to the amount of EGR. The increase in NIMEP here is due to an efficiency increase associated with boosting the engine - a behavior we believe is characteristic to this experimental apparatus.

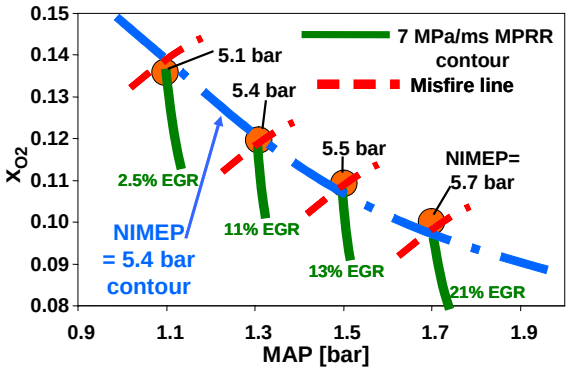

Fig. 12 High load limit points at different level of EGR; $T_{in} = 90^{o}$ C; $\lambda = 1$.

SUMMARY/CONCLUSIONS

The behavior of a boosted gasoline HCCI engine using Negative-Valve-Overlap at the high load limit was investigated. The maximum pressure rise rate (MPRR), which constrains the engine high load limit, is interpreted as proportional to the fuel energy density of the charge multiplied by an overall reaction rate ($1/\tau_{reaction}$). The effects on $1/\tau_{reaction}$ of the engine operating condition: manifold absolute pressure, EGR, and amount of residual were regressed in terms of the thermo-chemistry variables; See Eq. (4). The data scatter from this correlation (with $R^2 = 0.71$) was attributed to the effects of temperature and species concentration stratification. Not withstanding the stratification effects, the correlation is useful for scaling the MPRR values due to change of engine operating condition since it reflects the gross change of the thermo-chemistry variables.

The misfire limit at high load under different boost, intake temperature, and EGR was found to be tightly correlated to the thermo-chemistry variables; see Eq. (7). The tightness of the correlation (R^2=0.997) suggests that the misfire limit is not sensitive to the stratification details of the engine operation.

The amounts of boost, EGR, and residual gas need to be chosen to maximize the load (in terms of NIMEP) of an HCCI engine under the MPRR constraint. It was found that under such a constraint, the maximum load always occurs at the intersection between the constraining MPRR line of operation and the misfire boundary. The use of EGR shifts both the constant MPRR line and the misfire boundary so that the intersection is at a different operating point (in terms of the amount of boost and burned gas fraction in the unburned charge).

However, the NIMP does not change substantially between these points; thus under the MPRR constraint, the high load limit is approximately neutral to EGR.

REFERENCES

1. Homogeneous Charge Compression Ignition (HCCI) Engiens: Key Research and Development Issues, edited by F. Zhao et al, SAE International, Warrendale, PA, ISBN 0-7680-1123-X, 2003.
2. H. Santoso, J. Matthews and W. K. Cheng, "Managing SI/HCCI Dual-Mode Engine Operation," SAE Paper 2005-01-0162, 2005.
3. Y. Urata, M. Awasaka, J. Takanashi, T. Kakinuma, T. Hakozaki and A. Umemoto, "A Study of Gasoline-Fuelled HCCI Engine Equipped with an Electromagnetic Valve Train," 2004-01-1898.
4. C. Wildman, R.J. Scaring, W. Cheng, "On the Maximum Pressure Rise Rate in Boosted HCCI Operation," SAE Paper 2009-01-2727, 2009.
5. J. Hyvönen, G. Haraldsson, B. Johansson, "Supercharging HCCI to Extend the Operating Range in a Multi-Cylinder VCR-HCCI Engine," SAE Paper 2003-01-3214, 2003.
6. D. Yap, M.L. Wyszynski, A. Megaritis, H. Xu, "Applying boosting to gasoline HCCI operation with residual gas trapping," SAE Paper 2005-01-2121, 2005
7. M. Sjöberg, J. E. Dec, "EGR and Intake Boost for Managing HCCI Low-Temperature Heat Release over Wide Ranges of Engine Speed," SAE Paper 2007-01-0051, 2007.
8. T. Johansson, B. Johansson, P. Tunestål, H. Aulin, "HCCI Operating Range in a Turbo-charged Multi Cylinder Engine with VVT and Spray-Guided DI," SAE Paper 2009-01-0494, 2009.
9. J. Kamio, T. Kurotani, K. Kuzuoka, Y. Kuo, H. Taniguchi and K. Hashimoto, "Study on HCCI-SI Combustion Using Fuels Containing Ethanol," SAE Paper 2007-01-4051, 2007.
10. T. Kuboyama, Y. Moriyoshi, K. Hatamura, T. Yamada, J. Takanashi, "An Experimental Study of a Gasoline HCCI Engine Using athe Blow-Down Super Charge System," SAE Paper 2009-01-0496, 2009.
11. A. He, X., Donovan, M., Zigler, B., Palmer, T., Walton, S., Wooldridge, M., and Atreya, A., "An Experimental and Modeling Study of Iso-octane Ignition Delay Times Under Homogeneous Charge Compression Ignition Conditions," Combustion and Flame, Vol. 142, 2005, p.266-275.

CONTACT INFORMATION

Wai Cheng, Mail stop 31-165, MIT, Cambridge, MA 02139
email: wkcheng@mit.edu

ACKNOWLEDGMENTS

This research was funded by the US Department of Energy under a University Consortium on Low Temperature Combustion. The consortium members were MIT, U.C. Berkeley, U. of Michigan, and Stanford.

DEFINITIONS/ABBREVIATIONS

CA50
Crank angle at the 50% heat release point

EGR
Exhaust Gas Recirculation

LHV
Lower Heating Value of fuel by mass

$(LHV)_m$
Lower Heating Value of fuel by mole

MAP
Manifold Absolute Pressure

Load
Engine output as measured by NIMEP

m_f
Fuel mass per cycle

MON
Motor Octane Number

MPRR
Maximum Pressure Rise Rate

NIMEP
Net Indicated Mean Effective Pressure

N
Number of moles

NVO
Negative Valve Overlap

p
Pressure

$\dot{q}$
volumetric heat release

$\dot{Q}_L$
Total heat loss from charge

R
Universal gas constant

RON
Research Octane Number

T
Temperature

TDC
Top dead center

T_{exh}
Exhaust gas temperature

T_{in}
Intake fluid temperature

Total dilution
$(N_{EGR} + N_{excess\ fresh\ air} + N_{residual})/N_{charge}$

V
Volume

x_{burn}
Mole fraction of burned gas recirculation in unburned charge
$x_{burn} = x_r + x_{EGR}$

x_{EGR}
Mole fraction of Exhaust gas recirculation in unburned charge

X_{O2}
Mole fraction of oxygen in unburned charge

x_r
Mole fraction of residual gas in unburned charge

$\Delta\tau_{10\text{-}90}$
Time between 10% and 90% mass fraction burn

γ
Specific heat ratio

λ
Air-fuel equivalence ratio

$\tau_{reaction}$
Reaction time

APPENDIX A: RELATING x_r AND x_{EGR} TO x_{O2}

Let the cylinder content be consisted of N_r moles of residual, N_{EGR} moles of recirculated exhaust gas, N_a modes of air, and N_f modes of fuel. Then the number of moles of oxygen is:

$$N_{O_2} = x_{O_2}^b \left(N_r + N_{EGR}\right) + x_{O_2}^a N_a \quad \text{(A1)}$$

where $x_{O_2}^a$ and $x_{O_2}^b$ are respectively the mole fractions of oxygen in air and in the burned gas. (The former is 1/3.773; the latter is determined by the stoichiometry of combustion.) The total number of moles is:

$$N_{total} = N_a + N_f + N_r + N_{EGR} \quad \text{(A2)}$$

Therefore, the mole fraction of oxygen in the unburned charge is given by:

$$x_{O_2} = x_{O_2}^b \left(x_r + x_{EGR}\right) + x_{O_2}^a (1 - x_r - x_{EGR}) \frac{1}{1 + \left(W_a / W_f\right)/(A/F)} \quad \text{(A3)}$$

where W_a and W_f are the air and fuel molecular weights and A/F is the air-to-fuel mass ratio.

APPENDIX B: TOPOLOGY OF THE NIMEP AND MPRR CONTOUR LINES

The topology of the NIMEP and MPRR contours plotted with x_{O2} and MAP as the vertical and horizontal axes may be examined as follows. The NIMEP may be expressed as:

$$\text{NIMEP} = \frac{\text{MAP}}{RT_{in}} V_D \eta_{v,m} x_{O2} \left(\frac{x_f}{x_{O2}}\right)_S \frac{(LHV)_m}{\lambda} \eta_{f,i} \frac{1}{V_D} \quad \text{(B1)}$$

where R is the universal gas constant, T_{in} the intake fluid temperature, V_D the displacement volume, $\eta_{v,m}$ the volumetric efficiency based on the manifold condition, $(x_f/x_{O2})_s$ the stoichiometric fuel to oxygen molar ratio, λ the air equivalence ratio, $\eta_{f,i}$ the indicated net fuel conversion efficiency, and $(LHV)_m$ the fuel molar heating value. Thus the relationship between x_{O2} and MAP at constant NIMEP is given by:

$$x_{O2} = \frac{\text{NIMEP}}{\text{MAP}} \frac{RT_{in}}{\eta_{v,m}\eta_{f,i}\left(\frac{x_f}{x_{O2}}\right)_S \frac{(LHV)_m}{\lambda}} \quad \text{(B2)}$$

Since the η values do not change substantially, at a given T_{in} and λ, the NIMEP contours are approximately hyperbolas on the x_{O2} versus MAP plot. The slope of the contour may be measured by the logarithmic derivative

$$\left[\frac{d\ell n(x_{O2})}{d\ell n(\text{MAP})}\right]_{\text{NIMEP}} \approx -1 \quad \text{(B3)}$$

Thus along the constant NIMEP line, a 10% change in x_{O2} value would correspond to a 10% change in the MAP value; this assessment is consistent with the NIMEP contours depicted in Fig. 10.

The MPRR may be expressed via an overall reaction time $\tau_{reaction}$, as:

$$\text{MPRR} = \frac{1}{\tau_{reaction}} \frac{(\gamma - 1)\,\text{NIMEP}\;\; V_D}{\eta_{f,i} V_{CA50}} \quad \text{(B4)}$$

where the cylinder volume at 50% burn, V_{CA50}, is used to estimate the cylinder volume at the maximum pressure rise point in the cycle. Using Eq. (B1) to express NIMEP in terms of x_{O2} and MAP, Eq. (B4) becomes

$$\text{MPRR} = \frac{1}{\tau_{reaction}} \frac{(\gamma - 1)\;\; V_D}{\eta_{f,i} V_{CA50}} \left[\frac{\text{MAP}}{RT_{in}} V_D \eta_{v,m} x_{O2} \left(\frac{x_f}{x_{O2}}\right)_S \frac{(LHV)_m}{\lambda} \eta_{f,i} \frac{1}{V_D}\right] \quad \text{(B5)}$$

Thus the x_{O2}, MAP relationship along a MPRR contour is given by:

$$x_{O2} = \frac{MPRR}{MAP}\tau_{reaction}\frac{RT_{in}}{\eta_{v,m}\left(\frac{x_f}{x_{O2}}\right)_S\frac{\gamma-1}{\lambda}(LHV)_m\frac{V_D}{V_{CA50}}} \quad \text{(B6)}$$

Since $\eta_{v,m}$ and V_{CA50} do not significantly change, for a fixed T_{in} and λ, the slope of the MPRR contour on the x_{o2} versus MAP plot may be measured by:

$$\left[\frac{d\ell n(x_{O2})}{d\ell n(MAP)}\right]_{NIMEP} \approx -1 + \frac{d\ell n(\tau_{reaction})}{d\ell n(MAP)} \quad \text{(B7)}$$

Because $\tau_{reaction}$ decreases with MAP, Eq. (B7), together with Eq. (B3), indicate that the MPRR contour would be steeper (more negative) than the constant NIMEP contour.